The Minimal Detectable Bias for GNSS Observations with a Single Receiver Setup and a Geometry-Free Model

Peter F. de Bakker [(1)], Hans van der Marel [(1)], Peter J.G. Teunissen [(1,2)]
[(1)] *Delft University of Technology, The Netherlands*
[(2)] *Curtin University of Technology, Australia*

BIOGRAPHY

Peter de Bakker graduated in 2007 at the faculty of Aerospace Engineering from Delft University of Technology. He started as a PhD candidate at the Delft University of Technology in 2008 on the subject of precise point positioning and integrity monitoring.

Hans van der Marel is assistant professor at the Delft University of Technology, The Netherlands. He is currently involved in research on high precision GNSS positioning and navigation using GPS and Galileo, and scientific and meteorological applications of GNSS.

Peter Teunissen is Australian Research Council Federation Fellow at the Curtin University of Technology, Perth, Australia, and Professor of Earth Observation and Navigation at the Delft University of Technology, The Netherlands. He is the inventor of the LAMBDA method and has 25 years of GNSS research experience.

INTRODUCTION

In order to successfully use GNSS software under operational conditions, the software needs to be able to handle errors in the data. For this purpose a pre-processing step is usually added to the software to do a first screening of the data and to reduce the number of measurement errors that have to be handled during the final processing. During this pre-processing step the most severe irregularities in the data are detected and if necessary repaired. This makes the software more robust against errors that can occur under difficult conditions. Error detection can be implemented at receiver level as part of a Receiver Autonomous Integrity Monitoring (RAIM) algorithm. RAIM techniques are generally based on statistical tests that use the redundancy of the model to detect errors in the observation.

MINIMAL DETECTABLE BIAS

The Minimal Detectable Bias (MDB) is a measure for the size of the errors that can be detected with a certain power and probability of false alarm [1]. The MDB can be computed even before actual measurements have been carried out, using only a functional model and the expected stochastic properties of the data. In order to compute MDBs the type of error that is expected must be specified. In practice this means that MDBs are computed for different types of errors that can be expected in the data, such as outliers and slips in the data at different epochs. Therefore, the MDB is a very useful tool to assess the size of possible errors that can be detected, either during pre-processing of pseudo-range and carrier phase data, or in the final positioning, velocity and time computation step. Closed-form expressions are given for the MDBs of GPS data for single-baseline models in [2]. The impact of a weighted ionospheric pseudo observable is investigated in [3] and the impact of cross correlated observables in [4].

This contribution investigates the feasibility of error detection during pre-processing of GNSS data. For this reason the concept of RAIM and in particular internal reliability (quantified by the MDB) is applied to a single receiver geometry-free time differenced model, focusing on multi-frequency GPS and Galileo measurements. The MDB is defined as follows.

Under the null hypothesis H_0, biases are assumed absent and we have

$$H_0 : E\{y\} = Ax, D\{y\} = Q_y \qquad (1)$$

where E and D represent the expectation and dispersion, y is the vector of normally distributed observations with covariance matrix Q_y, A is the design matrix, and x is the vector of unknown parameters. For the alternative hypothesis H_a a bias vector b_y is introduced that defines the model error

$$H_a : E\{y\} = Ax + b_y, D\{y\} = Q_y \qquad (2)$$

The bias vector b_y can be decomposed in $C\nabla$, where C specifies the type of model error and ∇ is the size of the model error, or bias. C is used to specify in which observations the bias is present. The term bias here should not be confused with the more restrictive (and more or less constant) instrumental biases in the observations. In this paper a bias simply means a systematic error in the data as specified by the vector *C*. The term bias is used to distinguish it from purely stochastic errors in the data as specified by the co-variance matrix of the observations Q_y.

The generalized likelihood ratio test to test H_0 against H_a is [5]:

$$\text{reject } H_0 \text{ if } T_q > \chi^2_\alpha(q,0) \qquad (3)$$

where $\chi^2_\alpha(q,0)$ is the critical value for the chi-square distribution with q degrees of freedom and probability of false alarm α, and test statistic T_q:

$$T_q = \hat{e}^T Q_y^{-1} C \left(C^T Q_y^{-1} Q_{\hat{e}} Q_y^{-1} C \right)^{-1} C^T Q_y^{-1} \hat{e} \qquad (4)$$

where $\hat{e}$ is the least-squares residual vector and $Q_{\hat{e}}$ the corresponding covariance matrix. Under H_0 and H_a the statistic is distributed as follows:

$$\begin{aligned} H_0 &: T_q \sim \chi^2(q,0) \\ H_a &: T_q \sim \chi^2(q,\lambda) \end{aligned} \qquad (5)$$

with the non-centrality parameter λ:

$$\lambda = \nabla^T C^T Q_y^{-1} Q_{\hat{e}} Q_y^{-1} C \nabla \qquad (6)$$

The non-centrality parameter depends on the chosen detection power γ_0 and probability of false alarm α_0. The results in this paper are presented for $\gamma_0 = 0.80$ and $\alpha_0 = 0.001$, which gives $\lambda_0 \approx 17$. For many GNSS applications and especially for safety of life applications, γ will be set to a larger value and α will be set to a much smaller value. This will increase the value of λ, which in turn increases the MDBs on which it acts as a scale factor. For one-dimensional biases C is a vector and ∇ is a scalar known as the minimal detectable bias. For two or more-dimensional biases (6) describes an ellipse or (hyper)ellipsoid of bias combinations on the observations which can just be detected with the given power and probability of false alarm.

FUNCTIONAL MODEL

Two common models in GNSS processing are the geometry-based model and the geometry-free model. With the geometry-based model all receiver-satellite ranges are decomposed in three coordinate directions and the processing is performed for all satellites combined. With the geometry-free model the receiver-satellite ranges are not decomposed and processing is performed for each satellite separately. The geometry-based model generally has a higher redundancy than the geometry-free model which results in a stronger model. However, for the geometry-based model the satellite positions are required, while the geometry-free model does not use the satellite positions. This is an advantage for the geometry-free model: satellite orbit and clock data are not required and the processing is obviously also insensitive to mistakes in the satellite orbit and clock data, as well as tropospheric delay. An additional advantage of the geometry-free model is that, due to the single satellite approach, data from any GNSS can be processed without complications. This makes the geometry-free model very well suited for pre-processing techniques. Using a single receiver model also has the advantage that it can be implemented inside a GNSS receiver.

As mentioned before, the redundancy of the geometry-free model is generally not very high compared to the geometry-based model, because the observations are processed separately for each satellite. However, with the emergence of new and improved navigation systems and the upgrades of existing systems the number of observations made to one satellite is increased thus increasing the redundancy. A third frequency is added to the GPS system and the Galileo system will even use 4 frequencies. In this contribution the impact on reliability due to the increased number of available

frequencies and the improved code accuracy is investigated. The MDBs are computed using a range of realistic values for the variance and correlation of the observations.

For the geometry-free model, the observation equations for a single code C and phase L observation on carrier frequency i are as follows:

$$\begin{aligned} C &= g + \gamma_i I + \xi_C + \varepsilon_C \\ L &= g - \gamma_i I + \lambda A + \xi_L + \varepsilon_L \end{aligned} \qquad (7)$$

where g is a lumped parameter containing the receiver satellite range, the tropospheric delay and the clock biases, γ_i is the ionospheric dispersion factor equal to the carrier frequency of L1 squared divided by the carrier frequency of the observable under consideration squared (f_{L1}^2 / f_{Li}^2), I is the ionospheric delay on L1, λ the carrier wavelength, A the carrier phase ambiguity, ξ_C and ξ_L the code and phase instrumental and multipath delays and ε_C and ε_L the code and phase noise with $E\{\varepsilon_C\} = 0$ and $E\{\varepsilon_L\} = 0$.

For a single receiver setup, which is considered in this paper, the commonly used single or double differenced observations can obviously not be formed. This has a number of important drawbacks. Firstly, instrumental delays, which are eliminated in the double differenced observations, are not eliminated in a single receiver setup. Secondly, the ionospheric delay in the original observations is much larger than the ionospheric delay in the single difference between receivers. Therefore, for the single receiver setup a time differenced model is used instead to overcome these drawbacks. The time differenced model is comparable to assuming that the instrumental biases are constant in time (although certain linear combinations of instrumental biases will be absorbed by time-dependent parameters). Furthermore, in the time differenced model, the ionosphere fixed and weighted approaches are equivalent to assuming that the ionospheric delay is a constant or a zero mean velocity process. In a single difference model it is assumed that the differential ionospheric delay is zero or a zero mean process. This assumption is of course not applicable for a single receiver setup.

For time differenced processing, a first step is to use the time difference between two consecutive epochs. In this time difference many unknown parameters are eliminated from the observations. A second step is to use more epochs of data, a fixed window or all previous epochs, to detect biases. The MDB then depends also on the epoch at which the error occurs in the observations and the length of the data window.

In the difference between observations from two consecutive epochs, the multipath and instrumental delays ξ_C and ξ_L are greatly reduced and, under the null hypothesis, the carrier phase ambiguities are eliminated because they are constant as long as no cycleslip occurs [6]. This leaves the time differenced lumped parameter Δg and ionospheric delay ΔI:

$$\begin{aligned} E\{\Delta C\} &\approx \Delta g + \gamma \Delta I \\ E\{\Delta L\} &\approx \Delta g - \gamma \Delta I \end{aligned} \qquad (8)$$

Three different approaches of modelling the ionospheric delay are presented in this paper. With the ionosphere-constant approach the ionospheric delay is fixed to a constant value which is consequently eliminated from the time differenced observations:

$$E\left\{\begin{bmatrix} \Delta C \\ \Delta L \end{bmatrix}\right\} = \begin{bmatrix} 1 \\ 1 \end{bmatrix} \begin{bmatrix} \Delta g \end{bmatrix} \qquad (9)$$

With the ionosphere-float approach no constraint is put on the ionospheric delay. The time differenced ionospheric delay is estimated for each time difference in the model:

$$E\left\{\begin{bmatrix} \Delta C \\ \Delta L \end{bmatrix}\right\} = \begin{bmatrix} 1 & \gamma \\ 1 & -\gamma \end{bmatrix} \begin{bmatrix} \Delta g \\ \Delta I \end{bmatrix} \qquad (10)$$

With the ionosphere-weighted approach a pseudo observable for the time differenced ionospheric delay $\Delta \tilde{I}$ is added to the model:

$$E\left\{\begin{bmatrix} \Delta C \\ \Delta L \\ \Delta \tilde{I} \end{bmatrix}\right\} = \begin{bmatrix} 1 & \gamma \\ 1 & -\gamma \\ 0 & 1 \end{bmatrix} \begin{bmatrix} \Delta g \\ \Delta I \end{bmatrix} \qquad (11)$$

This pseudo observable can be based on an ionospheric model or it can be set to zero. The variance of this pseudo observable, which depends on the source of the observable, determines how restrictive the constraint on the time differenced ionospheric delay is. Two limiting cases are $D\{\Delta \tilde{I}\} \to 0$ and $D\{\Delta \tilde{I}\} \to \infty$ which makes the ionosphere-weighted model equivalent to the previously introduced ionosphere-fixed model and ionosphere-float model, respectively.

For dual frequency measurements, the time differenced ionosphere float model is very similar to the un-differenced ionosphere float model. For the other time differenced models, or more frequencies, equivalent models can be setup using un-differenced observations, which will then include extra parameters for instrumental biases and/or constant ionospheric delay (in case of ionosphere fixed).

STOCHASTIC MODEL

To determine the MDBs, an appropriate stochastic model must be defined to accompany the functional model. First the stochastic properties of the undifferened code and phase observables are defined. The stochastic properties of the time differenced GNSS observations can then be constructed from the undifferenced observations with the following operator:

$$D_\Delta = \mathbf{I}_{2n} \otimes \left(\begin{bmatrix} \mathbf{I}_{k-1} & \mathbf{0} \end{bmatrix} - \begin{bmatrix} \mathbf{0} & \mathbf{I}_{k-1} \end{bmatrix} \right) \qquad (12)$$

where $\otimes$ is the Kronecker product, $\mathbf{I}_i$ is an identity matrix of order i, k the number of epochs and $\mathbf{0}$ is a $k-1$ column vector with zeros, and n the number of frequencies. The covariance matrix of the time differenced code and phase observations is:

$$Q_\Delta = D_\Delta Q D_\Delta^T \qquad (13)$$

where Q is the covariance matrix of the undifferenced observations.

When the ionosphere-weighted approach (11) is used, the stochastic properties of the time differenced ionosphere pseudo observable $Q_{\Delta\tilde{I}}$ are appended to the covariance matrix of the time differenced observables Q_Δ of (13). In the time differenced processing, which is considered in this contribution, the following model for the ionosphere delay is used:

$$\begin{aligned} \Delta\tilde{I} &= \int_{t_{k-1}}^{t_k} \dot{I}(\tau) d\tau \\ \sigma^2_{\Delta\tilde{I}} &= \sigma^2_{\dot{I}} \Delta t \end{aligned} \qquad (14)$$

with $\dot{I}$ the derivative of the ionospheric delay and Δt the time interval. $\dot{I}$ is modeled as a white noise process [7], with $E\{\dot{I}(t)\} = 0$ ($E\{I(t)\} = \text{constant}$).

Also, there is no correlation between the GNSS measurements and the ionospheric pseudo observables.

In this paper, results are presented for different values for the variance of the ionosphere pseudo observable that span the range from the ionosphere-float to the ionosphere-fixed model. The standard deviation of the time differenced ionospheric pseudo observable depends on the temporal variation in ionospheric delay, the first time derivative in particular, and the time difference between the observations. The value for this standard deviation can be determined by analyzing estimated time differenced ionospheric delays using actual data. For the exploratory computations presented in this paper a representative value for moderate ionospheric conditions at mid-latitude was determined. Under these conditions the time derivative of the ionospheric delay on GNSS signals was found to be less than $1 mm/s$ on average with a standard deviation in the order of $1 mm/s$.

Table 1 shows the standard deviations of the code and phase observables that have been used in this paper as a starting point. However, for some specific results the standard deviation of the code observables has also been varied to show the impact of the code precision on the MDBs. The values in table 1 were taken from [8] and it has been assumed that the performance of the GPS L5 signal will be comparable to the Galileo E5a signal.

Table 1. Standard deviation of undifferenced observables

	GPS			Galileo				
	L1	L2	L5	E1	E5a	E5b	E5	E6
Code (cm)	15	15	3.9	6.1	3.9	3.7	0.9	4.4
Phase (mm)	1.0	1.3	1.3	1.0	1.3	1.3	1.3	1.2

All results in this paper are presented for a stochastic model *without* correlation between the observations unless *explicitly* stated otherwise. Two types of correlation between the observables have been considered: time correlation of the code measurements and cross-correlation between the phase measurements. Occurrences of these types of correlation on the observations from GNSS receivers were presented in e.g. [6] and [9].

The code observations are assumed to be exponentially correlated in time (see e.g. [10]), with a constant variance. For k epochs this gives the following dispersion for each code observable i:

$$D\left\{\begin{bmatrix} Ci(1) \\ Ci(2) \\ \vdots \\ Ci(k) \end{bmatrix}\right\} = Q_{Ci} = \sigma_{Ci}^2 \begin{bmatrix} 1 & \beta & \cdots & \beta^{k-1} \\ \beta & 1 & \cdots & \beta^{k-2} \\ \vdots & \vdots & \ddots & \vdots \\ \beta^{k-1} & \beta^{k-2} & \cdots & 1 \end{bmatrix} \quad (15)$$

where σ_{Ci} is the standard deviation of code observable i and β is the time correlation coefficient. If there is no time correlation ($\beta = 0$), the dispersion of the code observables simplifies to $\sigma_C^2 \mathbf{I}_k$, but $Q_{\Delta Ci}$ will still be a non diagonal matrix. Since no cross correlation between the code observables is considered, the Q_C matrix of all code observations is a block-diagonal matrix, with elements $Q_{C1} \ldots Q_{Cn}$.

The phase observables are assumed to be uncorrelated in time (for a measurement rate of 1Hz, this is a valid assumption if no smoothing is applied [6]). However, for some types of receivers cross correlation between the phase observables cannot be neglected [9]. When cross correlation is not neglected, this results in the following covariance matrix for the phase observations.

$$Q_L = \begin{bmatrix} Q_{L1} & Q_{L1L2} & \cdots & Q_{L1Ln} \\ Q_{L1L2} & Q_{L2} & \cdots & Q_{L2Ln} \\ \vdots & \vdots & \ddots & \vdots \\ Q_{L1Ln} & Q_{L2Ln} & \cdots & Q_{Ln} \end{bmatrix} \quad (16)$$

where $Q_{LiLj} = \rho_{LiLj} \sigma_{Li} \sigma_{Lj} \mathbf{I}_k$ with $i, j = 1, \ldots, n$. When there is no cross correlation, the covariance matrix of the phase observations simplifies to a block-diagonal matrix with elements $\sigma_{L1}^2 \mathbf{I}_k \ldots \sigma_{Ln}^2 \mathbf{I}_k$.

Assuming that the cross correlation between code and phase measurements can be neglected, the Q matrix of all undifferenced code and phase observations is a block-diagonal matrix, with elements Q_C and Q_L. The covariance matrix of the time differenced code and phase observables can now be constructed from (13).

TIME- VERSUS UNDIFFERENCED

In this paper a time-differenced approach was chosen in order to eliminate carrier phase ambiguities and time constant instrumental biases from the observation equations.

The advantages of the time differenced model compared to equivalent undifferenced models are:

- More compact model; no ambiguity terms, no instrumental biases; no constant ionosphere
- Hypotheses for slips become conventional alternative hypotheses (outliers)
- It is straightforward to model ionospheric delays as a zero mean process in the derivative

The disadvantage is of-course that in case of un-correlated GNSS observations, time correlation in the time differenced GNSS measurements is introduced. However, in case the observations already have time correlation this is not a disadvantage.

Typical for the time-differenced processing is also the sliding window approach, or finite window length. The minimum window length is 2, the maximum length is the length of the data segment, but in practice the window length can be much shorter as is shown in our results.

MODEL ERRORS

Several types of model errors can be considered.

- A slip in the phase observations of a single frequency. C then becomes a vector, which contains in the time differenced model only zeros except for a one at the entry that corresponds to the frequency and time differenced observation where the slip occurs.
- A simultaneous slip in the phase observations of each of the tracked frequencies. This corresponds to a momentary loss of lock of the receiver. C is now a matrix with a column for each tracked frequency, with each column containing one non-zero entry corresponding to the appropriate frequency and time differenced observation.
- An error in model of the time differenced ionospheric delay. For the ionosphere-weighted approach this is an error in the time differenced ionospheric-pseudo observable (C is a vector with zeros and a one corresponding to the biased pseudo observation); for the ionosphere-fixed approach this corresponds to an incorrect assumption of constant ionospheric delay (C is a vector with ionospheric dispersion factors γ).
- An outlier on a single code observation. C again becomes a vector, which contains only zeros except for a one at the entry that corresponds to the code observable and time difference right before the outlier directly followed by a minus one entry.

In this contribution only the first three types of model errors are considered..

RESULTS AND DISCUSSION

L1 carrier phase slip at the current epoch

Figures 1 and 2 show the MDB of a slip in the L1 carrier phase observation at the current epoch for respectively the ionosphere float and ionosphere fixed model, using different combinations of code and carrier phase data, and as function of the window length. There is a clear improvement in real-time bias detection, in other words decreasing MDBs with increasing number of used epochs (window length) and available frequencies. After the initial sharp decrease of the MDBs with increasing window length, the decrease becomes much more gradual for larger window sizes. Therefore, the use of a short window length will generally suffice, thereby limiting the required processing power.

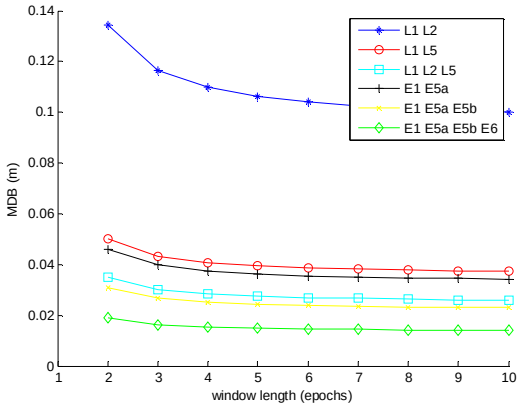

Fig 1. MDB for a slip on L1 for the ionosphere float model versus the number of epochs.

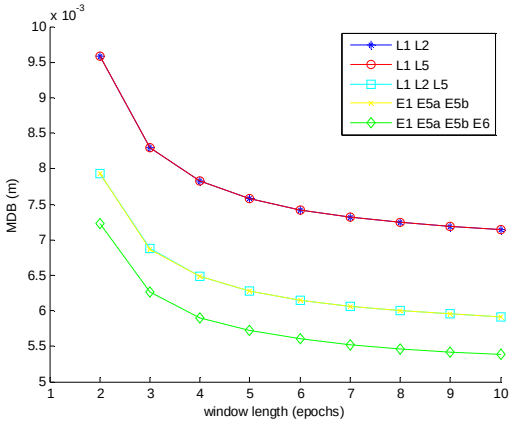

Fig 2. MDB a slips on L1 for the ionosphere fixed model versus the number of epochs.

The combinations of three and four frequencies perform significantly better than the dual frequency combinations, as can be expected because in the time differenced model the number of unknown parameters does not depend on the number of frequencies. The GPS L1 L2 combination for the ionosphere float model, figure 1, performs significantly worse than the L1 L5 combination due to the low precision of the L2 code compared to L5, which cannot be compensated by the smaller ionospheric dispersion factor for L2. On the other hand, in the ionosphere fixed model, figure 2, the precision of the code observables has almost no impact on the MDBs. Also, the frequencies of the carrier waves play no role because the dispersion factors are removed with the ionospheric delay. For the ionosphere-fixed model, combined with a one-dimensional error and dual frequency data, the MDBs only depend on the more precise phase observables, which can be explained as follows. The number of time differenced phase observations is $n(k-1)$ for n frequencies and k epochs. For the ionosphere-fixed model and a one-dimensional bias the number of unknown parameters is k ($k-1$ time differenced geometric terms and 1 bias). This means that for $k \geq 2$ there are sufficient time differenced carrier phase observables to compute all unknown parameters including the MDBs under investigation.

For the ionosphere-float model the number of unknown parameters is $2(k-1)+1$ and the dispersion factors *are* present in this model, thereby complicating the results. For dual frequency data, the number of unknown parameters is always larger than the number of time differenced carrier phase observables by 1, meaning that the MDBs depend to some extend on the code observations. The impact of the dual frequency code precision on the MDBs for the ionosphere-float model is further investigated in figure 3.

Figure 3 displays the impact of the precision of the code observations on the MDB for two dual frequency combinations L1 L2 and L1 L5. Three different values for the standard deviation of the L1 code observable have been considered. The horizontal axis indicates the standard deviation of the code observable of the second frequency and the vertical axis shows the size of the MDB for a slip on the L1 frequency. The values for the standard deviation of the code observables depend on the satellite elevation in combination with the receiver antenna gain and the code under consideration. On the one hand, a (future) GNSS signal with a high code rate, tracked from a satellite with a high elevation angle, could have a standard deviation of the code observable in the order of a few centimeters. On the other hand, the GPS C/A code tracked from a satellite with a low elevation angle could have a standard deviation of a few decimeters. Close inspection of the lines in figure 3

reveals that, when the standard deviation of the code observations of the second frequency is significantly smaller than the standard deviation of the code observations of the L1 frequency, the actual value of the code standard deviation for the L1 frequency is of little importance. This indicates that the size of the MDB is mostly determined by the standard deviation of the code observable with the highest precision. Also it is clear that the MDBs for L1 L5 are larger than for L1 L2 if the standard deviation for the L2 and L5 code are equal. This is because the ionospheric dispersion factor for L5 is higher than for L2 (1.79 respectively 1.65), which has a positive impact on the determination of the ionospheric delay, but a negative effect on the determination of the lumped parameter Δg and on the MDBs. This effect is shown in more detail later.

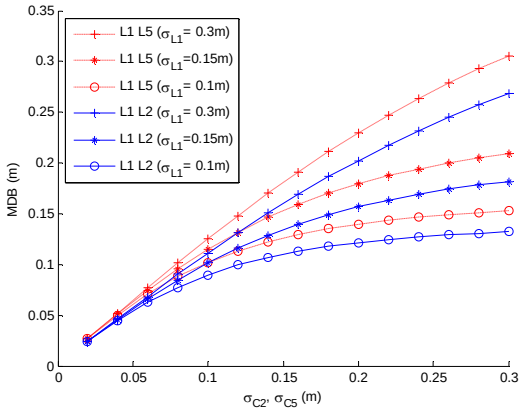

Fig 3. MDB for a slip on L1 for the ionosphere float model as a function of the precision of the code for the second frequency.

Figure 4 shows the MDB for the ionosphere weighted model for various values of the standard deviation of the time differenced ionospheric pseudo observable. As mentioned before, the ionosphere-weighted model has two limiting cases: for very precise ionosphere pseudo observations the ionosphere-weighted model behaves like the ionosphere-fixed model and for very imprecise pseudo observations it behaves like the ionosphere-float model. This is very clearly shown in figure 4 where the MDB for a slip on the first frequency is displayed versus the standard deviation of the time differenced ionospheric pseudo observable. At the right side of the figure the pseudo observable is assumed to have a very low precision and the MDBs have the same size as for the ionosphere-float model. When the standard deviation of the pseudo observable decreases to the order of the standard deviation of the code observables, the MDBs start to drop significantly. When the pseudo observable reaches the precision of the phase observables, the MDBs get close to the level of the ionosphere-fixed model and do not decrease any further. As mentioned before, for moderate conditions, the noise on the time derivative of the ionospheric delay is in the order of 1mm/s. This means that for $\Delta t = 1s$ the ionosphere-weighted model will be close to the ionosphere-fixed model for the purpose of cycleslip detection. When a measurement time interval of 30s or 60s is used, the weighted model behaves much like the ionosphere-float model but, especially for dual frequency GPS data, the MDB is still significantly smaller than for the ionosphere-float model. For a measurement time interval of more than a few minutes, using the ionosphere-weighted model no longer gives an advantage over the ionosphere-float model.

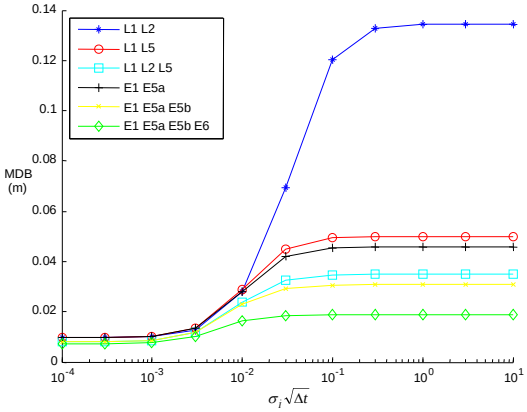

Fig 4. MDB for a slip on L1 for the ionosphere weighted model versus the precision of the ionospheric pseudo observable.

The ionospheric pseudo observable itself can also contain an error. This could be the occurrence of heavy scintillation or the passage of a travelling ionospheric disturbance (TID). Under these conditions the model of equation (14) is no longer valid. The MDB in the pseudo observable is shown in figure 5 as a function of $\sigma_{\Delta\tilde{I}}$. When the standard deviation of the pseudo observable increases beyond 3 cm, the MDB increases with a constant ratio for all signal combinations, this ratio is simply the square root of the non-centrality parameter λ.

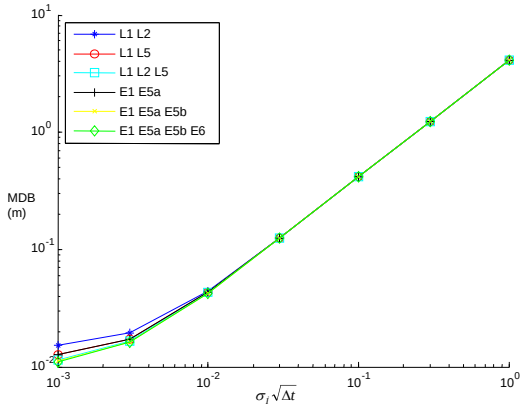

Fig 5. MDB for an error in the time differenced ionospheric pseudo observable versus the precision of the ionospheric pseudo observable.

In figure 6 the dotted lines show the effect of time correlation of the code observations on the MDB. A value of β=0.5 is used in equation (15) for the time correlation coefficient between consecutive epochs of 1Hz data [6]. Positive time correlation decreases the variance of the time differenced observations, thereby decreasing the MDB. If the time correlation is a result of smoothing, the improvement in the MDB can be compared to the improvement that an increase in the number of observations would have, since one smoothed observation is actually based on a number of 'raw' observations. This improvement diminishes when the number of epochs in the model is increased.

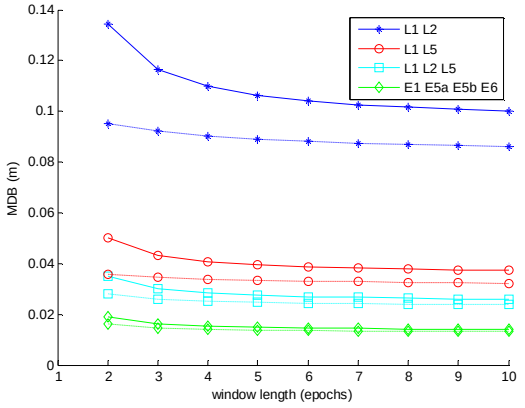

Fig 6. The impact of time correlation of the code observations on the MDB for a slip on L1 (solid without correlation; dotted with correlation of β=0.5).

L1 carrier phase slips at previous epochs

Figure 7 illustrates the effect on the MDB for the ionosphere float model of the epoch at which the error occurs l relative to the current epoch k. The most challenging situation is real-time error detection, where the error occurs at the current epoch ($l = k$), as was shown in figure 1. Comparison of the line for $l = k$ and the line for $l = k - 1$ shows that an error in the current epoch, that can just be detected with a large window size, can be detected one epoch later with a window size of only 4 epochs. This shows how challenging real-time detection is compared to near real-time detection. Therefore, if near real-time detection is acceptable for the application at hand, this could be a way to increase detection performance and decrease the computational burden.

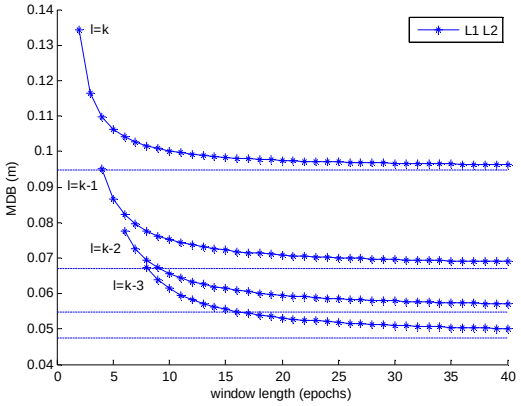

Fig 7. MDB for a slip on L1 for the ionosphere float model versus the number of epochs k and for different epochs at which the error occurs l.

Carrier phase slips at other frequencies

So far only carrier phase slips on the L1 frequency were considered. For a carrier phase slip on a different frequency the results are very similar. However, the actual values will depend on the carrier frequency combination and the carrier frequency on which the slip occurs.

Figure 8 shows the MDB for a slip on one of the phase observables of dual frequency data as a function of the carrier frequencies. The solid lines show the MDB for a slip on the first carrier phase observable which is displayed in the legend. The horizontal axis shows the frequency of the second carrier phase observable. The line corresponding to the L2 phase observable shows that the MDB has a minimum value when the second phase observable has the same frequency. This would correspond to a receiver tracking two identical, but independent signals from the same satellite. The MDB increases with increasing distance between the two frequencies, which results in the largest MDBs in

the figure for a carrier frequency combination including L1 and E5a.

The dotted lines show the MDB for the same carrier frequency combinations, but now for a slip on the second phase observable. Careful inspection of the figure reveals that for a given frequency combination the MDB is largest for a slip on the lowest frequency (largest dispersion factor γ).

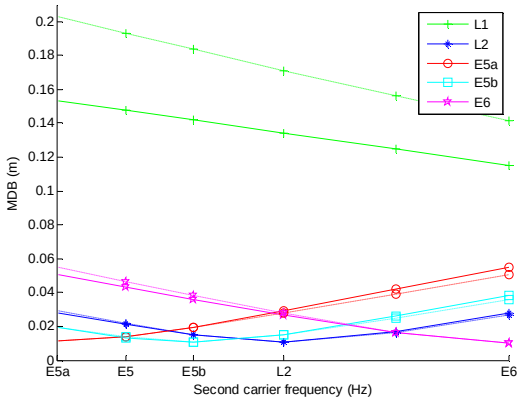

Fig 8. MDB for a slip on the first (solid) *or* second (dotted) phase observable of dual frequency data as a function of the carrier frequency of the second phase observable. The carrier frequency of the first phase observable is given in the legend.

Carrier phase slips on multiple frequencies

In this section, simultaneous slips on all tracked phase observables are considered. This type of error corresponds to a momentary loss of lock of a receiver tracking a satellite, that can e.g. result from signal blockage. As mentioned before, C now becomes a matrix with a column for each of the tracked frequencies. This results not in a single value for the MDB, but in an ellipse or (hyper)ellipsoid, depending on the number of frequencies, described by equation (6).

The principal axes of the ellipse or hyper(ellipsoid) can be determined by an eigenvalue decomposition of $\left(C^T Q_y^{-1} Q_{\hat{e}} Q_y^{-1} C\right)^{-1}$. The eigenvectors then give the principal axes and the MDB along these axes is equal to the square root of the eigenvalue times the non-centrality parameter λ.

Figure 9 and table 2 show results for the MDB ellipse for a simultaneous slip on both frequencies of dual frequency data. Figure 9 shows that the MDB ellipse is very elongated, showing that certain combinations of simultaneous biases on L1 and L2 are more difficult to detect than others. The first column in table 2 gives the standard deviation of the time differenced ionospheric pseudo-observation and its two limiting cases: ionosphere float and ionosphere fixed. The elongation of the ellipse is displayed in the right most column showing the semimajor axis of the ellipse divided by the semiminor axis. The MDB along the major axis and the direction of the major axis are displayed in column two and three, respectively. For the ionosphere-float model considered here, the weakest direction for error detection is given by the unit vector $(0.62, 0.79)^T$. In this direction a bias of 7.27 m can just be detected with the chosen power and probability of false alarm. This result reveals a important weak point of cycleslip detection with an ionosphere-float model. After a momentary loss of lock to a satellite, specific combinations of simultaneous slips can be present in the receiver data which are very difficult to detect.

The weakest direction for cycleslip detection depends on the ionospheric dispersion factors γ. A combination of slips of unknown size on both phase observables of dual frequency data with a time differenced model, is comparable to an undifferenced model with unknown phase ambiguities. The directions of the principal axis of the ellipses presented in table 2 are therefore closely related to those pertaining to the well-known linear combinations used for ambiguity float estimation.

For the ionosphere-weighted approach, the MDB ellipse shrinks and becomes less elongated when the precision of the ionospheric pseudo observable increases. The weakest direction also changes slowly, until it becomes equal to the line $\nabla_{L1} = \nabla_{L2}$ for the ionosphere-fixed model. At this point the uncertainty in the lumped parameter Δg becomes the dominant factor instead of the uncertainty in the ionospheric delay ΔI. This uncertainty, which again results in a very elongated ellipse, impacts each of the phase observables identically, resulting in the weakest direction for cycleslip detection given by $\nabla_{L1} = \nabla_{L2}$ for this situation.

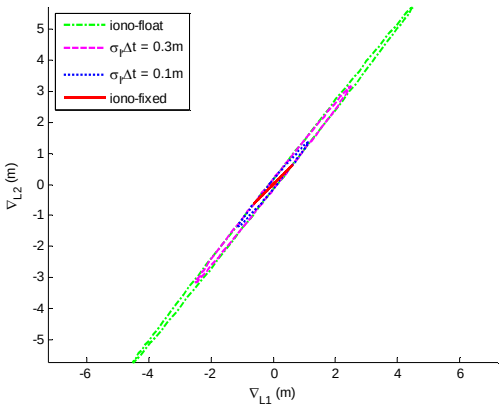

Fig 9. MDB ellipse of a simultaneous slip on both frequencies of GPS L1 L2 data for different ionospheric models.

Tables 3 and 4 display similar results as table 2 but now for, respectively, three and four frequency data. Only the major axis is presented in this paper because in this direction the largest undetected slips can occur and the improvement in this direction resulting from the ionospheric pseudo observable is most important. Analogous to the two dimensional case the weakest direction for the ionosphere-fixed model is along the line $\nabla_{Li} = \nabla_{L1}$ for $i = 1 \ldots n$. When the precision of the ionospheric pseudo observable increases the elongation of the ellipsoid first decreases significantly and finally increases slightly again when the model starts to behave as the ionosphere-fixed model.

Table 2. Two dimensional MDB ellipses

$\sigma_{\Delta\tilde{I}}$ (m/s)	$\max(\|\nabla\|)$ (m)	direction major axis $(L1, L2)^T$	$\frac{\max(\|\nabla\|)}{\min(\|\nabla\|)}$
float	7.2697	$(0.62, 0.79)^T$	69
1	6.6122	$(0.62, 0.79)^T$	63
0.3	4.0199	$(0.62, 0.78)^T$	39
0.1	1.7548	$(0.64, 0.77)^T$	19
0.03	0.9916	$(0.69, 0.73)^T$	20
0.01	0.8900	$(0.70, 0.71)^T$	45
0.003	0.8777	$(0.71, 0.71)^T$	99
0.001	0.8766	$(0.71, 0.71)^T$	125
fixed	0.8765	$(0.71, 0.71)^T$	129

Table 3. Three dimensional MDB ellipsoids

$\sigma_{\Delta\tilde{I}}$ (m/s)	$\max(\|\nabla\|)$ (m)	direction major axis $(L1, L2, L5)^T$	$\frac{\max(\|\nabla\|)}{\min(\|\nabla\|)}$
float	6.3597	$(0.49, 0.60, 0.63)^T$	841
1	6.1363	$(0.49, 0.60, 0.63)^T$	811
0.3	4.7020	$(0.49, 0.60, 0.63)^T$	622
0.1	2.2065	$(0.49, 0.60, 0.63)^T$	292
0.03	0.7829	$(0.51, 0.60, 0.62)^T$	103
0.01	0.4363	$(0.55, 0.59, 0.59)^T$	58
0.003	0.3769	$(0.57, 0.58, 0.58)^T$	50
0.001	0.3712	$(0.58, 0.58, 0.58)^T$	54
fixed	0.3705	$(0.58, 0.58, 0.58)^T$	57

Table 4. Four dimensional MDB hyper-ellipsoids

$\sigma_{\Delta\tilde{I}}$ (m/s)	$\max(\|\nabla\|)$ (m)	direction major axis $(E1, E5a, E5b, E6)^T$	$\frac{\max(\|\nabla\|)}{\min(\|\nabla\|)}$
float	3.1742	$(0.42, 0.54, 0.53, 0.50)^T$	451
1	3.1509	$(0.42, 0.54, 0.53, 0.50)^T$	448
0.3	2.9393	$(0.42, 0.54, 0.53, 0.50)^T$	418
0.1	2.0136	$(0.42, 0.54, 0.53, 0.50)^T$	286
0.03	0.7913	$(0.43, 0.54, 0.53, 0.50)^T$	112
0.01	0.3585	$(0.46, 0.52, 0.52, 0.50)^T$	51
0.003	0.2623	$(0.49, 0.50, 0.50, 0.50)^T$	37
0.001	0.2521	$(0.50, 0.50, 0.50, 0.50)^T$	38
fixed	0.2508	$(0.50, 0.50, 0.50, 0.50)^T$	40

Impact of cross correlation

In figure 10 the impact of cross correlation ($\rho_{LiLj} = 0.9$) of the phase observations is presented. Comparison of the dotted lines (with cross correlation) to the solid lines (without cross correlation) reveals that the MDBs for three or more frequencies decrease if the phase observables are cross correlated.

This decrease of the MDB for cross correlated phase observations, does not occur for more dimensional errors. The direction of and MDB along the principal axis of the triple frequency MDB ellipsoids displayed in table 2 are, in fact, not impacted at all by cross correlation of the phase observables. The shape of the ellipsoid *does* change and becomes even more elongated for cross correlated phase data. This means that errors in directions different from the principal axis can be detected more easily when the phase observables are cross correlated. However, it is important to note that strong correlation between the observables might well influence the type of errors that will occur on the data. Therefore, one should not jump to the conclusion that cross correlation improves error detection.

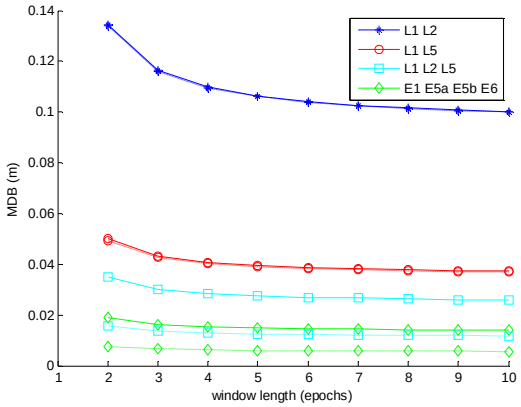

Fig 10. The impact of cross correlation of the phase observations on the MDB for a slip on L1 (solid without correlation; dotted with correlation).

CONCLUSIONS

In this paper the impact of additional GNSS frequencies and improved code accuracy on the minimal detectable biases for a single receiver time differenced geometry-free model has been presented. The single receiver time differenced geometry-free model is well suited for a pre-processing step for GNSS software, and can be implemented inside a GNSS receiver for on-the-fly bias detection.

The size of model errors that can be detected with a certain power and level of significance (quantified by the MDB) decreases with increasing number of used epochs and available frequencies, as expected. Increased precision of the code observables improves the MDBs for the ionosphere float model, but have almost no impact on the MDBs for the ionosphere-fixed model. This was explained by an analysis of the redundancy of the model. If there are more phase observations than unknown parameters, the code observations are not needed for the bias detection. The size of the MDB in the ionosphere float model is mostly determined by the standard deviation of the code observable with the highest precision.

To bridge the gap between the ionosphere-float and ionosphere-fixed model, an ionosphere-weighted model was introduced, with a time differenced ionospheric pseudo observable. For representative values of the standard deviation of the time differenced ionospheric pseudo observable and a measurement interval of $1s$, the MDBs for the ionosphere-weighted model are comparable to ionosphere-fixed values. For a measurement interval of $30s$ the MDBs for the ionosphere-weighted model are still significantly smaller than for the ionosphere-float model. For a measurement interval of a few minutes the ionosphere-weighted model performs equal to the ionosphere-float model.

This paper demonstrated the challenging nature of real-time detection compared to near real-time detection. The MDB for a bias in the current epoch using a very large window length is equal to the MDB for a bias in the previous epoch using a window length of only 4 epochs. Therefore, if a slight delay in detection is acceptable for a certain application, the detection performance can be increased for a given window length, or the window length can be decreased, consequently decreasing the computational burden, for a given detection performance.

The hypothesis of a simultaneous slip on each phase observable of multi-frequency GNSS data was shown to give a very elongated MDB ellipse or (hyper)ellipsoid with the ionosphere-float model. These very elongated ellipses reveal a weak point of cycleslip detection with an ionosphere-float model because specific combinations of slips, which can be present in the receiver data after a momentary loss of lock to a satellite, are very difficult to detect. One way to remedy this shortcoming, which is related to the uncertainty in the ionospheric delay, is to use an ionosphere-weighted model. For an ionosphere-weighted approach, the MDB ellipse shrinks when the precision of the ionospheric pseudo observable increases.

For optimal performance of a cycleslip detection algorithm, including slip combinations that are difficult to detect, it is advisable to use an ionosphere-weighted model in combination with a short time interval between the measurements.

REFERENCES

[1] Baarda, W. (1968). *A testing procedure for use in geodetic networks.* Netherlands Geodetic Commission, Publications on Geodesy, New Series, 2(5).

[2] Teunissen, P.J.G. (1998). Minimal detectable biases of GPS data. *Journal of Geodesy 72*, 236-244.

[3] De Jong, K. and P.J.G. Teunissen (2000) Minimal Detectable Biases of GPS observations for a weighted ionosphere. *Earth, Planets and Space 52*, 857-862.

[4] De Jong, K. (2000) Minimal Detectable Biases of Cross-Correlated GPS Observations. *GPS Solutions 3*, 12-18.

[5] Teunissen, P.J.G. (2006). *Testing theory; an introduction.* Delft VSSD, 2nd ed.

[6] De Bakker, P.F., H. van der Marel, C.C.J.M. Tiberius (2009). Geometry-free undifferenced, single and double differenced analysis of single

frequency GPS, EGNOS and GIOVE-A/B measurements. *GPS Solutions* DOI: 10.1007/s10291-009-0123-6.
[7] Teunissen, P.J.G. (2001). *Dynamic Data Processing*, Delft VSSD, 1st ed.
[8] De Wilde, W., F. Wilms, A. Simsky, J. Sleewaegen (2006). Early performance results for new Galileo and GPS signals-in-space. In Proceedings of ENC GNSS, 2006. Manchester.
[9] Amiri-Simkooei, A.R. and C.C.J.M. Tiberius (2007). Assessing receiver noise using GPS short baseline time series. *GPS Solutions 11(1)*, 21–35.
[10] Strang, G. and K. Borre (1997). *Linear algebra, geodesy, and GPS.* Wellesly-Cambridge Press.